Preprints of the 20th World Congress
The International Federation of Automatic Control
Toulouse, France, July 9-14, 2017

Multiple Fault-Tolerant In-Wheel Vehicle Control Based on High-level Control Reconfiguration ⋆

András Mihály ** **Péter Gáspár** ** **Balázs Németh** *

* *Institute for Computer Science and Control Hungarian Academy of Sciences, Budapest, Hungary*
** *Institute for Computer Science and Control Hungarian Academy of Sciences and MTA-BME Control Engineering Research Group, Budapest, Hungary*

Abstract:
The paper deals with the fault-tolerant reconfigurable control design of a four-wheel independently-actuated (4WIA) electric vehicle. The purpose of the proposed method is to ensure the velocity and path tracking of the 4WIA vehicle in the event of a fault or performance degradation in one or even several in-wheel electric motors. The novelty of the presented method is the high-level control reallocation method based on the Linear Parameter Varying (LPV) control framework, by which the torque vectoring and steering of the vehicle are modified in order to deal with the impact of faulty in-wheel motors. The operation of the designed fault-tolerant method is validated in CarSim simulation environment.

Keywords: in-wheel vehicle, 4WIA vehicle, reconfigurable control, trajectory tracking.

1. INTRODUCTION

As the popularity of hybrid/electric vehicles grows, researchers and automotive companies increasingly focus on developing in-wheel electric vehicles. One of the most promising features of a 4WIA vehicle from a vehicle dynamic point of view is its capability to realize precise torque vectoring, which enhances the stability and maneuverability of the vehicle, see Wu et al. (2013); Shuai et al. (2013); Xiong et al. (2012); Castro et al. (2012). By applying energy optimal torque distribution and higher efficiency regenerative braking compared to regular electric vehicles, the range of 4WIA electric vehicles can also be increased, see Cheng and Xu (2015); Wang et al. (2011, 2014); Ringdorfer and Horn (2011).

Earlier papers have already discussed the issues of fault detection and fault-tolerant control strategies for ground vehicles, see Németh et al. (2012); Bodson (2002); Johansen and Fossen (2013). However, due to the complexity and dynamic behavior of in-wheel vehicles equipped with four independent electric hub motors even more attention is required on fault-tolerant control design, since a faulty hub motor can degrade the performance or even destabilize the motion of 4WIA vehicles. Hence, some of the research focuses on the fault-tolerant design of the wheel hub motor itself to guarantee an adequate level of performance following a failure, as proposed by Ifedi et al. (2013). The automatic reallocation of in-wheel motor torques during a fault-event was proposed by Wang and Wang (2012), where a sliding mode high-level controller and a quadratic programming allocation method handled the distribution of wheel torques. Li et al. (2016) also introduced a sliding mode controller, but with the aim of rearranging the steering geometry according to the in-wheel motor fault location. A robust $\mathcal{H}_\infty$ yaw rate tracking controller based on the well-known bicycle model was presented in Jing et al. (2015) considering the performance degradation of the active steering system and the in-wheel motors. In Hu et al. (2015), an interesting fault-tolerant method was introduced to handle the effect of electric steering system failure, generating steering angle by applying differential drive torque with the front in-wheel motors.

The present paper introduces a novel high-level control reconfiguration method based on a nonlinear four-wheel vehicle model and LPV framework, with the aim of handling faults or performance degradation in one or even several in-wheel motors of the vehicle. The novelty of the proposed method lies in the high-level control design with reconfiguration properties, which makes it possible to deal with the effect of in-wheel motor failures without using computationally cumbersome constrained optimization techniques.

The paper is organized as follows: Section 2 presents the control-oriented nonlinear two-track vehicle model. Section 3 details the robust and fault-tolerant reconfigurable trajectory tracking control design method based on LPV framework and shows the implementation scheme. Section 4 demonstrates the operation of the reconfigurable controller in case of different in-wheel motor failures in CarSim simulation environment.

⋆ The research was supported by the National Research, Development and Innovation Fund through the project "SEPPAC: Safety and Economic Platform for Partially Automated Commercial vehicles" (VKSZ 14-1-2015-0125). This paper was supported by the János Bolyai Research Scholarship of the Hungarian Academy of Sciences.

2. VEHICLE MODEL FOR TRAJECTORY TRACKING

The aim of the control design is to guarantee both velocity and path tracking for the in-wheel electric vehicle. Thus, the longitudinal and lateral dynamics of the vehicle are considered, while the vertical motion is ignored. The motion equation of the vehicle is based on the reduced nonlinear two-track bicycle model, see Figure 1.

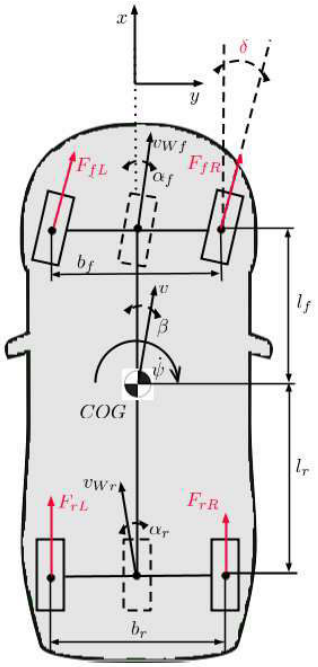

Fig. 1. Nonlinear two-track bycicle model

The detailed derivation of the motion equations in the planar plane is given in Kiencke and Nielsen (2005). The state variables used in this description are the vehicle velocity v, the side-slip angle β and the vehicle yaw rate $\dot{\psi}$. Assuming the tire cornering stiffness to be equal for all wheels, the differential equations of the vehicle motion are the following:

$$\begin{aligned} m\dot{v} =&(F_{fL}+F_{fR})\cos(\delta-\beta)+(F_{rL}+F_{rR})\cos\beta \\ &-c_w\rho A\frac{v^2}{2}\cos\beta-2c\alpha_f\sin(\delta-\beta)+2c\alpha_r\sin\beta \end{aligned} \tag{1}$$

$$\begin{aligned} mv\dot{\beta} =&2c\alpha_f\cos(\delta-\beta)+(F_{fL}+F_{fR})\sin(\delta-\beta) \\ &-\dot{\psi}mv-(F_{rL}+F_{rR}-c_w\rho A\frac{v^2}{2})\sin\beta \\ &+2c\alpha_r\cos\beta \end{aligned} \tag{2}$$

$$\begin{aligned} J\ddot{\psi} =&(l_f-n\cos\delta)(F_{fL}+F_{fR})\sin\delta+\frac{b_r}{2}(F_{rR}-F_{rL}) \\ &+(l_f-n\cos\delta)2c\alpha_f\cos\delta-(l_f+n)2c\alpha_r \\ &+\frac{b_f}{2}(F_{fR}-F_{fL})\cos\delta \end{aligned} \tag{3}$$

where m is the total vehicle mass, J is the yaw inertia, l_f and l_r are geometric parameters related to the front and rear axle positions, b_f and b_r are the front and rear track width, n is the dynamic caster, c_w is the drag co-efficient, ρ is the air mass density, A is the frontal area contact surface of the vehicle, c is the cornering stiffness of the tires, $\alpha_f=\delta-\beta-\dot{\psi}l_f/\dot{\xi}$ and $\alpha_r=-\beta+\dot{\psi}l_r/\dot{\xi}$ are the side slip angles of the front and rear wheels. The front steer angle is noted with δ, while the longitudinal wheel forces with F_{ij}, $i\in[f=front, r=rear]$, $j\in[L=left, R=right]$.

In order to reduce the complexity of the model equations in (1)-(3), approximation is used assuming the steering angle δ and side slip angle β to be small. Thus, the motion equations are simplified by substituting $\cos\delta\cong 1$, $\cos\beta\cong 1$, $\cos(\delta-\beta)\cong 1$, $\sin\delta\cong\delta$ and $\sin(\delta-\beta)\cong\delta-\beta$. Hence

$$\begin{aligned} m\dot{v} =&F_{fL}+F_{fR}+F_{rL}+F_{rR}-c_w\rho A\frac{v^2}{2} \\ &-2c\alpha_f(\delta-\beta)+2c\alpha_r\beta \end{aligned} \tag{4}$$

$$\begin{aligned} mv\dot{\beta} =&2c\alpha_f+(F_{fL}+F_{fR})(\delta-\beta) \\ &-(F_{rL}+F_{rR}-c_w\rho A\frac{v^2}{2})\beta+2c\alpha_r-mv\dot{\psi} \end{aligned} \tag{5}$$

$$\begin{aligned} J\ddot{\psi} =&(l_f-n)(F_{fL}+F_{fR})\delta+\frac{b_r}{2}(F_{rR}-F_{rL}) \\ &+(l_f-n)2c\alpha_f+\frac{b_f}{2}(F_{fR}-F_{fL})-(l_r+n)2c\alpha_r) \end{aligned} \tag{6}$$

The nonlinear model can be written in a state space form as follows:

$$\begin{aligned} \dot{x} &= A(x,u)x+B(x,u)u \\ y &= Cx \end{aligned} \tag{7}$$

where the state vector of the system is $x=\begin{bmatrix}v & \beta & \dot{\psi}\end{bmatrix}^T$. The control inputs are the longitudinal wheel forces F_{ij} and the steering angle δ, which are given in the input vector $u=[F_{fL}\ F_{fR}\ F_{rL}\ F_{rR}\ \delta]^T$. The measured outputs are the vehicle speed and yaw rate, i.e., $y=\begin{bmatrix}v & \dot{\psi}\end{bmatrix}^T$.

3. LPV CONTROL DESIGN

To the nonlinear planar plane model of the 4WIA vehicle introduced in Section 2 a gain scheduling LPV controller is a possible solution. Since velocity and path tracking of the in-wheel vehicle are both required, it is necessary to define two reference signals. The reference signal for the vehicle lateral control is the reference yaw rate $\dot{\psi}_{ref}$, which is calculated based on the driver steering input δ_d. A possible expression is $\dot{\psi}_{ref}=v/d\cdot e^{-\frac{t}{\tau}}\cdot\delta_d$, which depends on the velocity, vehicle geometry parameters, understeer gradient and the time delay, see Rajamani (2005). For the longitudinal motion control a desired velocity $\dot{\xi}_{ref}$ is also given by the driver to follow. These two reference signals are formulated in a reference vector $R=[\dot{\xi}_{ref}\ \dot{\psi}_{ref}]^T$.

The vehicle model described by (7) is dependent on the vehicle states and the steering input as well. The vehicle states v and $\dot{\psi}$ are assumed to be measured by widespread wheel speed sensors and a gyroscope, while β can not be measured directly with cheap sensors but can be estimated based on vehicle measurements. Most of the β estimation methods are based on applying observers (Extended Kalman Filter, Sliding-mode observer, etc.) as discussed in Baffet et al. (2009); Grip et al. (2009); Bevly et al. (2009). A combined method of model observer and direct integration method introduced in Fukada (1999) has been applied to mass product vehicles and proven to be robust

in real life situations. Moreover, utilizing GPS/INS can enhance the efficiency of side-slip estimation, as described in Leung et al. (2011); Ryu et al. (2002). The steering angle δ can also be easily measured with a steering angle sensor.

The scheduling variables are $\rho_1 = v$, $\rho_2 = \beta$, $\rho_3 = \dot{\psi}$ and $\rho_4 = \delta$, $\rho_5 = 1/v$ and $\rho_6 = 1/v^2$. Denoting

$$\rho = [\rho_1 \ \rho_2 \ \rho_3 \ \rho_4 \ \rho_5 \ \rho_6]^T,$$

the nonlinear vehicle model can be rewritten as an LPV model as follows:

$$\begin{aligned} \dot{x} &= A(\rho)x + B(\rho)u \\ y &= Cx \end{aligned} \tag{8}$$

In order to consider faulty in-wheel motors and design a reconfigurable LPV controller for such cases, four monitoring parameters $\sigma_{ij} \in [0 \quad 1]$, $i \in [f, r]$, $j \in [L, R]$ are also introduced for each in-wheel motors of the vehicle. These monitoring parameters represent the level of healthiness, i.e., $\sigma_{ij} = 1$ implies a healthy motor, while $\sigma_{ij} = 0$ represents a complete engine failure. Note that a certain level of performance degradation can also be represented by the monitoring parameters. Denoting

$$\sigma = [\sigma_{fL} \ \sigma_{fR} \ \sigma_{rL} \ \sigma_{rR}]^T,$$

a gain scheduling LPV controller is designed with the scheduling variables defined in vector ρ and σ.

As both velocity and path tracking are aims of the control design, two reference signals given in reference vector R must be tracked. The velocity error $z_v = |\dot{v}_{ref} - \dot{v}|$ must be minimized with the optimization criterion: $z_v \to 0$. At the same time, yaw rate error between the reference signal and the actual yaw rate $z_{\dot{\psi}} = |\dot{\psi}_{ref} - \dot{\psi}|$ must also be minimized with the optimization criterion $z_{\dot{\psi}} \to 0$. Hence, a performance vector is given as

$$z_1 = \begin{bmatrix} z_v \ z_{\dot{\psi}} \end{bmatrix}^T. \tag{9}$$

The maximum possible outputs of the in-wheel motors and the steer-by-wire steering system are defined by their physical construction limits. Considering these limits, a second performance vector is formulated as

$$z_2 = [F_{fL} \ F_{fR} \ F_{rL} \ F_{rR} \ \delta]^T, \tag{10}$$

with the aim to avoid saturation of the actuators.

3.1 High-level controller design

The proposed high-level controller is based on a weighting strategy formulated through a closed-loop P-K-Δ structure, as depicted in Figure 2. P is the augmented plant in which uncertainties given by Δ are taken into consideration, while K is the controller.

The control design method is based on constructing weighting functions considering control objectives, disturbances and sensor noises. Note that despite of these weighting functions being formulated in frequency domain, their state-space representation forms are applied in the control design.

Weighting functions W_p scale two tracking errors defined in z_1. These weighting functions can be considered as penalty functions, thus weights should be large where small signals are desired and vice versa. The purpose of

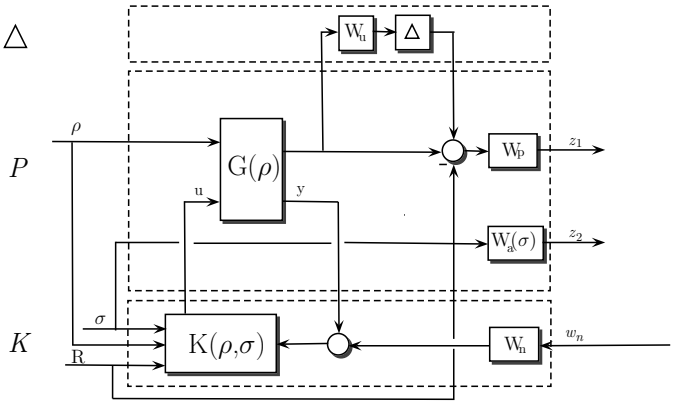

Fig. 2. Closed-loop interconnection structure

the weighting function W_n is to consider sensor noises, the neglected dynamics is represented by the weighting function W_u, while W_a is responsible for the control allocation and reconfiguration between actuators in case of fault events.

In order to achieve a robust reconfigurable fault-tolerant controller, the design of the weighting function W_a is essential and is in the main focus of the paper. The goal of the design is to ensure an optimal split between steering and the drive/brake torques generated by the four in-wheel motors, even in case of engine faults or performance degradations.

This criterion is realized by the scheduling parameters σ_{ij}, scaling the actuators of the 4WIA vehicle based on their healthiness levels. Thus, the weighting function of the steering is given as

$$W_{a\delta} = min(\sigma_{ij})/(\delta_{max}\chi_1), \tag{11}$$

while the torque generation of the four in-wheel motors are represented by

$$W_{aF_{ij}} = (T_{zmax}\chi_2)/(\sigma_{ij}), \tag{12}$$

where δ_{max} and T_{zmax} represent the maximum steering angle and maximum in-wheel motor torque, while χ_1 and χ_2 are design parameters tuned to achieve the desired control allocation.

Hence, in case of an in-wheel motor failure or performance degradation, weighting function $W_{aF_{ij}}$ corresponding to the location of the given motor is altered through the value of the monitoring parameter σ_{ij} in such a way that it penalizes the use of the given in-wheel motor and reallocates the control inputs to the healthy actuators, i.e., the steering system and the healthy in-wheel motors. Therefore even multiple in-wheel motor failures can be handled, which is one of the biggest advantages of the presented method.

The LPV control approach is based on using parameter-dependent Lyapunov functions as suggested by Bokor and Balas (2005); Wu et al. (1996). The quadratic LPV performance problem is to select the parameter-varying controller in a manner that ensures the quadratic stability of the resulting closed-loop system and at the same time guarantee that the induced $\mathcal{L}_2$ norm from the disturbance w to the performances z is less than the value γ.

The minimization task is the following:

$$\inf_{K} \sup_{\varrho \in \mathcal{F}_{\mathcal{P}}} \sup_{\|w\|_2 \neq 0, w \in \mathcal{L}_2} \frac{\|z\|_2}{\|w\|_2} \leq \gamma. \tag{13}$$

Linear Matrix Inequalities (LMIs) based solution is given for the quadratic LPV γ-performance problem.

3.2 Control Architecture

The reconfigurable control system is implemented in a hierarchical structure. The architecture of the two-layer, reconfigurable control system is depicted in Figure 3.

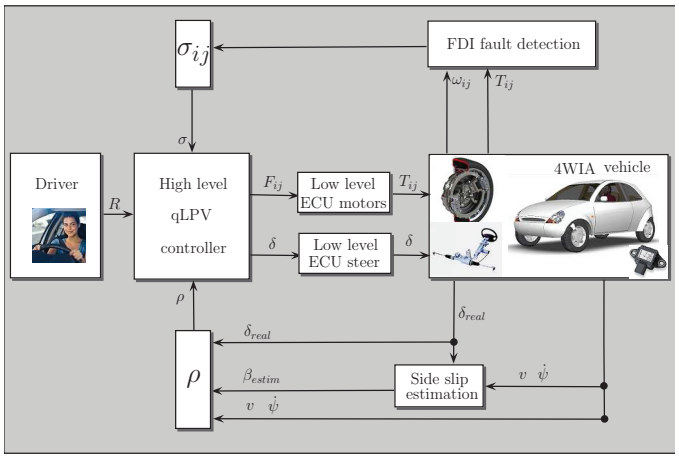

Fig. 3. Architecture of control system

The purpose of the high-level LPV controller is to calculate the desired control inputs, i.e., the steering angle and the four wheel forces. For this purpose the LPV controller calculates with the measured and estimated signals inserted in the scheduling vector ρ, and with the monitoring signals put in the scheduling vector σ.

The second layer of the hierarchical control structure is responsible for tracking the control signals by the low-level controllers, i.e., the steering system and the in-wheel motors of the 4WIA vehicle. Hence, these controllers transform the steering angle and the in-wheel motor torques into real physical parameters of the actuators. Here, steering is modeled as a first-order system as discussed in Takanori et al. (2004). Considering the much faster torque response of the in-wheel motors compared to the dynamic response of the wheels, it can be modeled as a second-order system (see Tahami et al. (2003)) given by the following transfer function:

$$T_{ij}^{m}(s) = \frac{T_{ij}(s)(1+\eta)}{1+2\zeta+2\zeta^2} \tag{14}$$

where $T_{ij} = R_{eff} F_{ij}$ are the control torques given by the high-level LPV controller, T_{ij}^{m} are the real output torques of the in-wheel motors, ζ and η are parameters related to the response time and steady state error of the electric hub motors.

4. SIMULATION RESULTS

The simulation vehicle is a small 4WIA vehicle equipped with a steer-by-wire steering system. The in-wheel motors are assumed to have the specifications of state-of-the-art technology, see in Table 1. The main geometric, dynamic and mass parameters of the simulated 4WIA vehicle are shown in Table 2.

Table 1. In-wheel motor parameters

Parameter	Value	Unit
Total motor mass	34	kg
Peak output power	75	kW
Continuous output power	54	kW
Peak output torque	1000	Nm
Continuous output torque	650	Nm
Nominal input voltage range	$200-400$	Vdc

Table 2. Vehicle parameters

Parameter	Value	Unit
Vehicle mass (m)	830	kg
Yaw moment of inertia (J)	1110.9	kgm^2
Distance from C.G to front axle (l_f)	1.103	m
Distance from C.G to rear axle (l_r)	1.244	m
Tread front (b_f)	1.416	m
Tread rear (b_r)	1.375	m
Dynamic caster (n)	0.045	m
Wheel cornering stiffness (c)	30	kN/rad
Aerodynamic drag co-efficient (c_w)	0.343	$-$
Front contact surface (A)	1.6	m^2

The simulation task for the in-wheel vehicle is to follow the trajectory of the S-turn shown in Figure 4. The reference velocity is set to constant 60 km/h (see Figure 5(a)), while the reference yaw rate is given by the driver based on its steering input, as illustrated in Figure 5(b). During the simulation the vehicle velocity, yaw rate, side slip angle and steering angle are measured with the built-in sensors of CarSim.

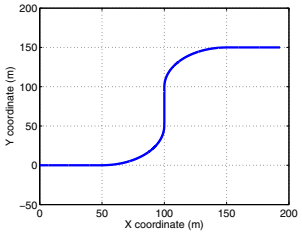

Fig. 4. Reference trajectory

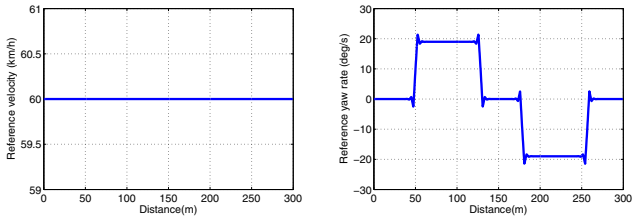

(a) Reference velocity (b) Reference yaw rate

Fig. 5. Reference velocity and yaw rate

4.1 Operation of the fault tolerant method

Three simulation cases have been evaluated in order to demonstrate the operation of the presented fault-tolerant

method. In the first corner all of the in-wheel motors are fully functional, while in front of the second corner three different kinds of fault events are considered. First, only the front left (fL fault) in-wheel motor fault is simulated, the second case assumes both the front left and rear right (fL-rR fault) motors to fail, while in the third case all of the in-wheel motors fail except for the rear left one (fL-fR-rR fault).

The high-level control signals of the LPV controller are shown in Figure 6. It is well demonstrated that as more and more in-wheel motors fail at the second corner the prescribed differential wheel forces are reduced by the controller (see Figure 6(a)-Figure 6(c)), while the steering angle increases significantly.

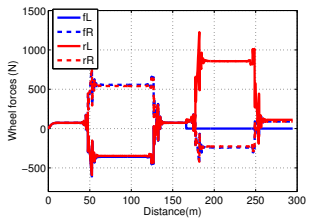

(a) Wheel forces: fL fault

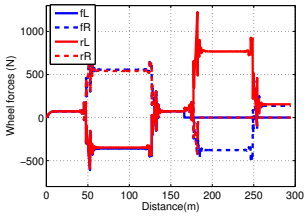

(b) Wheel forces: fL-rR fault

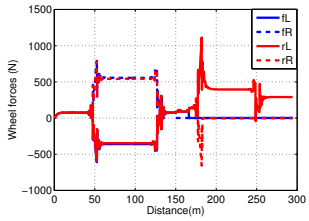

(c) Wheel forces: fL-fR-rR fault

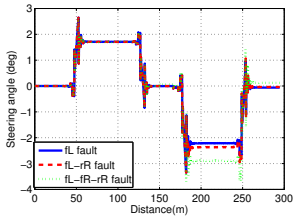

(d) Actuated steering angle

Fig. 6. High-level control signals

The low-level control signals depicted in Figure 7 correspond to the high-level signals, showing that the increasing number of in-wheel motor faults decreases differential torque generation of the in-wheel motors (see Figure 7(a)-Figure 7(c)). Hence, for the second cornering maneuver the vehicle is reconfigured in such a way that it follows the curve with steering intervention rather than torque vectoring.

The model scheduling variables of the of the high-level LPV controller inserted in vector ρ are shown in Figure 8 for the three simulation cases. The measured vehicle velocity ρ_1 depicted in Figure 8(a) remains around the given reference, while the side slip angle ρ_2 shown in Figure 8(b) decreases as more in-wheel faults occur and steering intervention is preferred over torque vectoring. The measured vehicle yaw rate ρ_3 in Figure 8(c) remains steady even during control reconfiguration induced by the motor faults.

The fault monitoring and controller scheduling parameters inserted in vector σ are shown in Figure 9. Note that for better demonstrating the effect of control reconfiguration during fault events only fully healthy ($\sigma_{ij} = 1$) and fully inoperational ($\sigma_{ij} = 0$) in-wheel motors are demonstrated. It can be seen that the value of the monitoring parameter σ_{fl} in Figure 9(a) drops from 1 to 0 in all three cases, since the front left electric motor of the vehicle is assumed

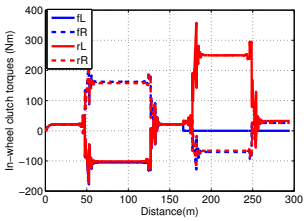

(a) Motor torques: fL fault

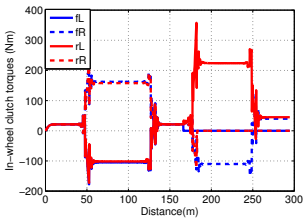

(b) Motor torques: fL-rR fault

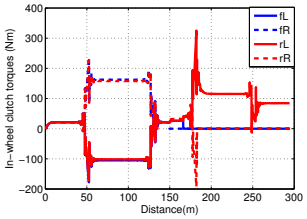

(c) Motor torques: fL-fR-rR fault

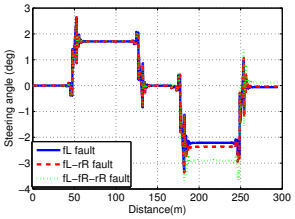

(d) Steering angle

Fig. 7. Low-level control signals

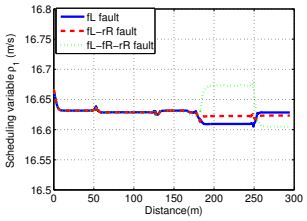

(a) ρ_1

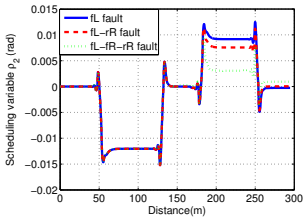

(b) ρ_2

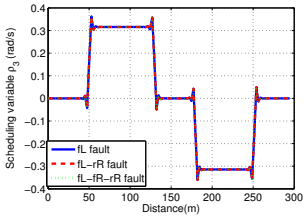

(c) ρ_3

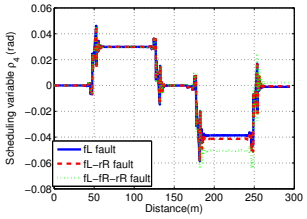

(d) ρ_4

Fig. 8. Scheduling variables ρ of the LPV model

to fail in every simulation case. On the other hand, monitoring parameter σ_{rl} in Figure 9(c) remains 1 in all cases, representing the healthy in-wheel engine for all three cases.

The performances of the reconfiguration method are shown in Figure 10. The velocity error depicted in Figure 10(a) stays within 1 km/h even during multiple in-wheel faults, while yaw rate error shown in Figure 10(b) also remains acceptable.

5. CONCLUSION

The paper has presented a multiple fault-tolerant LPV control method for 4WIA vehicles with a steer-by-wire steering system. The proposed strategy is based on a high-level control reconfiguration method, in which the detected in-wheel motor faults are represented by monitoring parameters also used as scheduling variables for the controller. The operation of the proposed trajectory tracking control method has been demonstrated during cornering

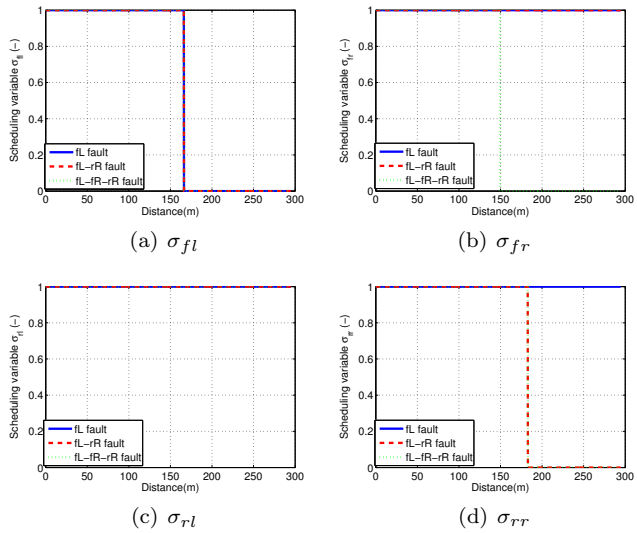

(a) σ_{fl} (b) σ_{fr}

(c) σ_{rl} (d) σ_{rr}

Fig. 9. Monitoring variables σ of the LPV model

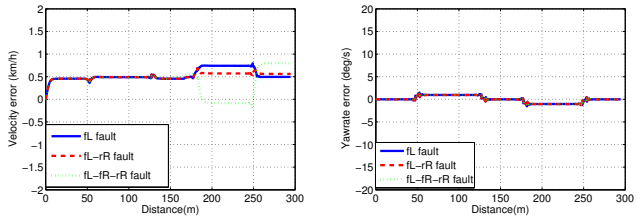

(a) Velocity error (b) Yaw-rate error

Fig. 10. Performances of the control method

maneuvers performed in CarSim simulation environment with a different number of fault events. It has been shown that the proposed reconfiguration method is capable of dealing with even multiple fault events.

REFERENCES

Baffet, G., Charara, A., and Lechner, D. (2009). Estimation of vehicle sideslip, tire forces and wheel cornering stiffness. *Control Engineering Practice*, 1255–1264.

Bevly, D., Ryu, J., and Gerdes, J. (2009). Estimation of vehicle sideslip, tire force and wheel cornering stiffness. *Control Engineering Practice*, 17, 1255–1264.

Bodson, M. (2002). Evaluation of optimization methods for control allocation. *Journal of Guidance, Control and Dynamics*, 25, 703–711.

Bokor, J. and Balas, G. (2005). Linear parameter varying systems: A geometric theory and applications. *16th IFAC World Congress, Prague*.

Castro, R., Araújo, R.E., Tanelli, M., Savaresi, S.M., and Freitas, D. (2012). Torque blending and wheel slip control in evs with in-wheel motors. *Vehicle System Dynamics*, 50, 71–94.

Cheng, C.L. and Xu, Z. (2015). Wheel torque distribution of four-wheel-drive electric vehicles based on multi-objective optimization. *Energies 2015*, 8, 3815–3831.

Fukada, Y. (1999). Slip-angle estimation for vehicle stability control. *Vehicle System Dynamics:International Journal of Vehicle Mechanics and Mobility*, 32, 375–388.

Grip, H.F., Imsland, L., Johansen, T.A., Kalkkuhl, J.C., and Suissa, A. (2009). Vehicle sideslip estimation. *IEEE Control Systems*, 29, 1–15.

Hu, C., Jing, H., Wang, R., Yan, F., Li, C., and Chen, N. (2015). Fault-tolerant control of FWIA electric ground vehicles with differential drive assisted steering. *9th IFAC Symp. Fault Detection, Supervision and Safety for Technical Processes*, 48, 1180–1185.

Ifedi, C., Mecrow, B., Brockway, S., Boast, G., Atkinson, G., and Kostic-Perovic, D. (2013). Fault tolerant in-wheel motor topologies for high performance electric vehicles. *IEEE Transactions on Industry Applications*, 49, 1249 – 1257.

Jing, H., Wang, R., Chadli, M., Hu, C., Yan, F., and Li, C. (2015). Fault-tolerant control of four-wheel independently actuated electric vehicles with active steering systems. *9th IFAC Symp. Fault Detection, Supervision and Safety for Technical Processes*, 48, 1165–1172.

Johansen, T. and Fossen, T. (2013). Control allocation - survey. *Automatica*, 49, 1087–1103.

Kiencke, U. and Nielsen, L. (2005). *Automotive Control Systems*. Springer, Verlag Berlin Heidelberg.

Leung, K.T., Whidborne, J.F., Purdy, D., and Dunoyer, A. (2011). A review of ground vehicle dynamic state estimations utilising gps/ins. *Vehicle System Dynamics:International Journal of Vehicle Mechanics and Mobility*, 49, 29–58.

Li, B., Du, H., and Li, W. (2016). Fault-tolerant control of electric vehicles with in-wheel motors using actuator-grouping sliding mode controllers. *Mechanical Systems and Signal Processing*, 72.

Németh, B., Gáspár, P., Bokor, J., Dugard, L., and Sename, O. (2012). Fault-tolerant control design for trajectory tracking in driver assistance systems. *8th IFAC Symp. Fault Detection, Supervision and Safety of Technical Processes*, 186–191.

Rajamani, R. (2005). *Vehicle Dynamics and Control*. Springer.

Ringdorfer, M. and Horn, M. (2011). Development of a wheel slip actuator controller for electric vehicles using energy recuperation and hydraulic brake control. *IEEE International Conference on Control Applications, Denver, USA*, 313–318.

Ryu, J., Rossetter, E.J., and Gerdes, J.C. (2002). Vehicle sideslip and roll parameter estimation using gps. *6th Int. Symposium on Advanced Vehicle Controly (AVEC 2002)*.

Shuai, Z., Zhang, H., Wang, J., Li, J., and Ouyang, M. (2013). Lateral motion control for four-wheel-independent-drive electric vehicles using optimal torque allocation and dynamic message priority scheduling. *Control Engineering Practice*, 24, 55–66.

Tahami, F., Kazemi, R., and Farhanghi, S. (2003). A novel driver assist stability system for all-wheel-drive electric vehicles. *IEEE Transactions on Vehicular Technology*, 52, 683–692.

Takanori, F., Shogo, M., Kenji, M., Norihiko, A., and Koichi, O. (2004). Active steering systems based on model reference adaptive nonlinear control. *Vehicle System Dynamics: International Journal of Vehicle Mechanics and Mobility*, 42, 301–318.

Wang, B., Huang, X., Wang, J., Guo, X., and Zhu, X. (2014). A robust wheel slip ratio control design combining hydraulic and regenerative braking systems for in-wheel-motors-driven electric vehicles. *Journal of the Franklin Institute*, 50, 71–94.

Wang, R., Chen, Y., Feng, D., Huang, X., and Wang, J. (2011). Development and performance characterization of an electric ground vehicle with independently actuated in-wheel motors. *Journal of Power Sources*, 196, 3962–3971.

Wang, R. and Wang, J. (2012). Fault-tolerant control for electric ground vehicles with independently-actuated in-wheel motors. *Journal of Dynamic Systems, Measurement, and Control*, 134.

Wu, F., Yang, X.H., Packard, A., and Becker, G. (1996). Induced l^2-norm control for LPV systems with bounded parameter variation rates. *Int. J. Nonlinear and Robust Control*, 6, 983–998.

Wu, F.K., Yeh, T.J., and Huang, C.F. (2013). Motor control and torque coordination of an electric vehicle actuated by two in-wheel motors. *Mechatronics*, 23, 46–60.

Xiong, L., Yu, Z., Wang, Y., Yang, C., and Meng, Y. (2012). Vehicle dynamics control of four in-wheel motor drive electric vehicle using gain scheduling based on tyre cornering stiffness estimation. *Vehicle System Dynamics*, 50, 831–846.